Science of the Total Environment 918 (2024) 170507

Contents lists available at ScienceDirect

Science of the Total Environment

journal homepage: www.elsevier.com/locate/scitotenv

Sources and transport of CO_2 in the karst system of Jiguan Cave, Funiu Mountains, China

Yidong Li [a,b], Yan Yang [a,c,*], Xianguo Wang [d], Weijun Luo [e], Jingyao Zhao [f], Zhe Sun [g], Zhimao Ye [a,c], Xiaomin Chen [a,c], Xiao Shi [a,c], Yanzhi Xu [h], Jonathan L. Baker [b]

[a] Chongqing Key Laboratory of Karst Environment, School of Geographical Sciences, Southwest University, Chongqing 400715, China
[b] Institute of Geology, University of Innsbruck, Innsbruck 6020, Austria
[c] Chongqing Jinfo Mountain Karst Ecosystem National Observation and Research Station, Chongqing 400715, China
[d] Henan Geological Engineering Survey Institute, Zhengzhou 450012, China
[e] State Key Laboratory of Environmental Geochemistry, Institute of Geochemistry, Chinese Academy of Sciences, Guiyang 550081, China
[f] Institute of Global Environmental Change, Xi'an Jiaotong University, Xi'an 710049, China
[g] Institute of Geography and Resources Science, Sichuan Normal University, Chengdu 610066, China
[h] Henan Jiguan Cave Tourism Development Limited, Luanchuan 471500, China

HIGHLIGHTS

- Seasonal signals of cave CO_2 result from soil dynamics and cold-season ventilation with variance from anthropogenic CO_2 superimposed.
- Human respiration modifies cave CO_2 and carbon-isotope composition.
- Heavy rainfall event results in a positive carbon-isotope shift via reduced soil CO_2 contribution to karst waters.

GRAPHICAL ABSTRACT

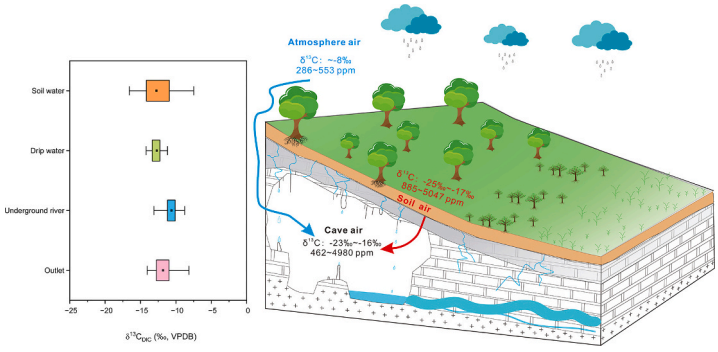

ARTICLE INFO

Editor: Christian Herrera

Keywords:
Carbon isotopes
Soil CO_2
Cave CO_2
Human activities
Karst system

ABSTRACT

Conveyance and modification of carbon-isotope signals within the karst system remain difficult to constrain, due to the complexity of interactions between multiple components, including precipitation, bedrock, soil, atmosphere, and biota. Cave monitoring is thus critical to understanding both their transport in the karst system and dependence on local hydroclimatic conditions. Jiguan Cave, located in Funiu Mountain in central China, is representative of karst tourist caves with relatively thin epikarst zone. We conducted a comprehensive monitoring program of cave climate from 2018 to 2021 and measured $\delta^{13}C$ during 2021 in monthly and heavy-rainfall samples of soil CO_2, cave CO_2, cave water (drip water and underground river), and underground river outlet. Our results demonstrate synchronous variations between CO_2 concentration and $\delta^{13}C_{CO2}$ in both soil and cave air on seasonal time scales. Cave pCO_2 and carbon-isotope composition further exhibited a high sensitivity to human respiration with fluctuations of ~2000–3000 ppm within 4 days during the cave closure period in July 2021

* Corresponding author at: Chongqing Key Laboratory of Karst Environment, School of Geographical Sciences, Southwest University, Chongqing 400715, China.
E-mail address: yy2954@swu.edu.cn (Y. Yang).

https://doi.org/10.1016/j.scitotenv.2024.170507
Received 12 October 2023; Received in revised form 23 January 2024; Accepted 25 January 2024
Available online 1 February 2024

without tourists. ^{13}C-depleted isotopic signal of cave air in summer is the mixture of human respiration and soil CO_2 which varies as a function of regional hydrological conditions of the summer monsoon during the rainy season with high temperatures and humidity. However, respired CO_2 from the overlying soil was expected to be the only principal source of the cave CO_2 when the anthropogenic CO_2 source was removed. The high seasonal amplitude of cave air $\delta^{13}C_{CO2}$ reflects ventilation dynamics, which leads to a prominent contribution from the external atmosphere during winter. Intriguingly, although the $\delta^{13}C$ signal reflects complex vertical processes in the vertical karst profile, a heavy summer rainfall event was related to anomalously high $\delta^{13}C$ values of cave water that can be utilized to interpret rainfall intensity and regional hydroclimate.

1. Introduction

The karst system is composed of the epikarst zone and subsurface cavities that facilitate the transfer of meteoric water and atmosphere through vegetation, soil, and bedrock toward groundwater reservoirs, including subterranean rivers and water traps (Covington, 2016; Wu et al., 2019). Extensive underground river networks and human-accessible caves provide a natural advantage for studying the processes of the subsurface carbon cycle through time and space (Liu et al., 2010; Yuan, 2015; Behzad et al., 2023). Modern process monitoring of carbon isotopes in concert with spatiotemporal variations of cave-air CO_2 in cave systems has the potential to improve the understanding of cave-carbon sources and sinks (Breecker et al., 2012; Cao et al., 2020, 2021; Druhan et al., 2021; Faimon et al., 2020; Mattey et al., 2021) and reveal transport mechanisms of climate information through the karst system (Oster et al., 2012; Treble et al., 2015; Breitenbach et al., 2015; Riechelmann et al., 2017; Li and Li, 2018; Li et al., 2021; Zhang et al., 2023).

The source of cave-air CO_2 is an important indicator of internal cave environment but has significant dynamic changes at multiple spatio-temporal scales (Spötl et al., 2005; Baldini et al., 2008; Cao et al., 2021; Liñán et al., 2023). Similar seasonal variations of cave pCO_2 have been observed in most caves, with low (high) values in winter (summer) (Banner et al., 2007; Frisia et al., 2011; Pu et al., 2017; Li and Li, 2018; Li et al., 2021). In general, the concentration of cave-air CO_2 derives from the balance of CO_2 inputs and outputs, principally through groundwater infiltration, speleothem deposition, and ventilation (Faimon et al., 2012, 2020; Lang et al., 2017). The standard model of secondary mineral formation and subsurface carbon cycling considers soil respiration as the main CO_2 source to the vadose zone (Hendy, 1971). Soil CO_2 dissolves in percolating water according to its partial pressure, and through a hydrolysis reaction, carbonic acid (H_2CO_3) is formed, which dissolves carbonate minerals to saturation during transport through the epikarst (Spötl et al., 2005; Banner et al., 2007; Li and Li, 2018). At the same time, soil CO_2 can migrate downward as a gas through the pipeline of fissures and conduits in the surface karst zone or as a result of cave air inflow resulting from low internal pressure, which 'pulls' soil air into the cave (Baldini et al., 2008; Frisia et al., 2011). On the other hand, several studies have highlighted the important contribution of sub-soil carbon sources to cave CO_2 in karst areas, including deep-rooted plant respiration (Breecker et al., 2012), biological respiration in bedrock fractures (Bergel et al., 2017), and the decomposition of organic matter (Atkinson, 1977; Mattey et al., 2016). In addition, drip and subsurface river degassing (Spötl et al., 2005; Breitenbach et al., 2015) and human respiration from tourism activities (Baker and Genty, 1998; Faimon et al., 2006; Lang et al., 2015; Liñán et al., 2023) constitute indirect CO_2 input fluxes that influence cave CO_2 variability.

The balance of cave CO_2 output and removal is mainly controlled by cave ventilation and depends on two factors: (1) the location and height of the cave entrance and the volume and geometry of the caverns; and (2) air circulation driven by temperature contrasts between the interior and exterior of the cave (Fairchild et al., 2006; Breecker et al., 2012; Breitenbach et al., 2015; Mattey et al., 2016, 2021; Lang et al., 2017; Kukuljan et al., 2021). Three ventilation modes can be summarized for multi-entrance caves (dynamic caves) based on airflow direction: (1) the downward airflow (DAF) mode, in which cave air flows from the upper entrance toward the lower entrance when external air temperature (T_{ext}) is warmer than internal cave-air temperature (T_{int}); (2) the upward airflow (UAF) mode, opposite the DAF mode when $T_{int} > T_{ext}$; (3) a transitional mode between these two modes (Faimon et al., 2012). Seasonal cave-air pCO_2 induced by different airflow modes directly controls drip pH and CO_2 degassing, which affects dripwater isotopic composition, elemental signatures, hydrogeochemistry, and ultimately calcite precipitation and speleothem growth rates (Banner et al., 2007; Mattey et al., 2008, 2021; Breitenbach et al., 2015; Li and Li, 2018; Cao et al., 2021). High-resolution monitoring of CO_2 changes in cave systems is thus necessary to investigate the potential impact of soil processes on cave pCO_2, determine the source of cave air CO_2 and quantify cave ventilation modes.

The carbon-isotope signal ($\delta^{13}C$) in karst systems can be influenced by multiple site-specific factors (Tooth and Fairchild, 2003; Lambert and Aharon, 2011; Riechelmann et al., 2017; Li and Li, 2018; Fohlmeister et al., 2020; Mattey et al., 2021; Yin et al., 2021). Regional temperature and precipitation influence the development and ecology of overlying soil vegetation, which modulates the CO_2 respiration rate yield of plant roots and microbes (Genty et al., 2003; Moreno et al., 2010; Mattey et al., 2016) and ultimately determines the proportion of carbon isotopes in soil-respired CO_2, with greater activity (high soil pCO_2) resulting in lower $\delta^{13}C_{CO2}$. Carbonate bedrock is dissolved along fractures by carbonic acid formed through a hydrolysis reaction with aqueous soil-derived CO_2 (Baker et al., 1997; Bar-Matthews et al., 2000). The degree of bedrock dissolution is further controlled by whether the karst system is nearer to 'open' or 'closed' end-member conditions—the latter of which results in a higher contribution from bedrock $\delta^{13}C$ (Hendy, 1971; Rudzka et al., 2011; Fohlmeister et al., 2011, 2020). When infiltrating water enters the cave to form a drip, CO_2 degasses from the drip due to cave ventilation effects and the difference between dripwater and cave-air pCO_2. Higher contrasts enhance degassing, which concomitantly increases dripwater pH, calcite saturation, and the growth rate of speleothems (Spötl et al., 2005; Baldini et al., 2008; Pu et al., 2017). Meanwhile, higher residence time, prior calcite precipitation (PCP), and low drip rate (associated with drier conditions overall) are important processes that increase the $\delta^{13}C$ value of dripwater DIC and speleothems above what is predicted from soil-bedrock interactions alone (Fairchild et al., 2012). Finally, the cave microclimate (temperature, humidity, and ventilation) and kinetic fractionation effects during precipitation can also lead to $\delta^{13}C$ offsets (Li et al., 2018; Fohlmeister et al., 2020; Mattey et al., 2021). Because these processes often co-exist and interact, the drivers of $\delta^{13}C$ variability in the karst system need to be carefully evaluated across relevant spatiotemporal scales.

In this study, monthly $\delta^{13}C$ data in the karst system and high-resolution pCO_2 in soil-air and cave-air are obtained to identify the sources of cave-air CO_2. In 2021, a brief cave closure from July 22 to July 25 and anomalously low visitor counts in August (~55 times lower than in previous years) was caused by extreme record-breaking precipitation (Nie and Sun, 2022) and pandemic policy restrictions, respectively. This window provided an opportunity to diagnose the impact of anthropogenic CO_2 on the composition of the cave air. Meanwhile, $\delta^{13}C$ sampling from the vertical profile of the karst system during a heavy rainfall event was conducted to explore the transport and modification

of $\delta^{13}C$ signals and the relationship with the local hydrology environment.

2. Study area

Jiguan Cave (33°46′N, 111°34′E) is located in the north slope of the Funiu Mountains (eastern Qinling Mountain remaining vein), about 4 km west of Luanchuan city in central China (Fig. 1). The study area lies within the transition zone between the humid and the semi-arid regions (Li et al., 2021), and the mean annual temperature and precipitation recorded by the meteorological station in Luanchuan were 13.0 °C and 819 mm (2010−2021), respectively. Due to the influence of the Asian monsoon, the wet season from April to September accounts for 76–94 % of the annual precipitation. The overlying bedrock mainly consists of Sinian chloritized marble with a thickness of 30–40 m (Li et al., 2021). Vegetation above the cave is dominated by secondary deciduous broad-leaved forest including conifers, oaks and bushes since ~1993. The soil overlying the cave is ~10 to 60 cm thick and derived from a mixture of wind-blown dust and weathered carbonate rock. The B horizon containing bedrock fragments is covered by a thin brown A horizon, which is rich in plant roots and residues (Fig. S1a).

The altitude of the cave entrance is ~900 m asl. and its length is ~5600 m (Sun et al., 2018). During the monitoring period from 2019 to 2021, the mean air temperature inside the cave was 16.4 °C with a range of 14.0–19.5 °C. Relative humidity remained >90 %, indicating that the internal environment is relatively stable. A previous study of oxygen isotopes showed that drip water $\delta^{18}O$ reflected precipitation from the most recent wet season (July–September) in ordinary years (Sun et al., 2018; Chen et al., 2023), while in drought years, it reflected the combination of wet-season precipitation and aquifer storage from prior years (Table S1).

Jiguan Cave is open for tourism 10 h per day year-round, except for a closure from July 22–25, 2021, caused by a record-breaking rainfall event that occurred in the Henan Province. Normally visitors enter the cave at intervals of 10–30 min, with an average annual visitor volume of ~554,000 from 2017 to 2019. The monthly distribution of visitors prior to 2020 ranges from a minimum in January (~1600–11,000 visitors/month) to a maximum in August (~124,000–184,000 visitors/month) (Fig. S2).

3. Materials and methods

3.1. Field sampling

Soil infiltration water was collected at a depth of ~20 cm (Fig. 1b) using a custom handmade collector (Fig. S1b), consisting of a polyethylene plate and bottle. The plate is 15 cm in diameter and 7 cm in height, covered with two layers of gauze to prevent mud and sand from entering. A 1000 ml collection bottle was connected to the bottom of the plate through silicone tubing. Another silicone tube was inserted into

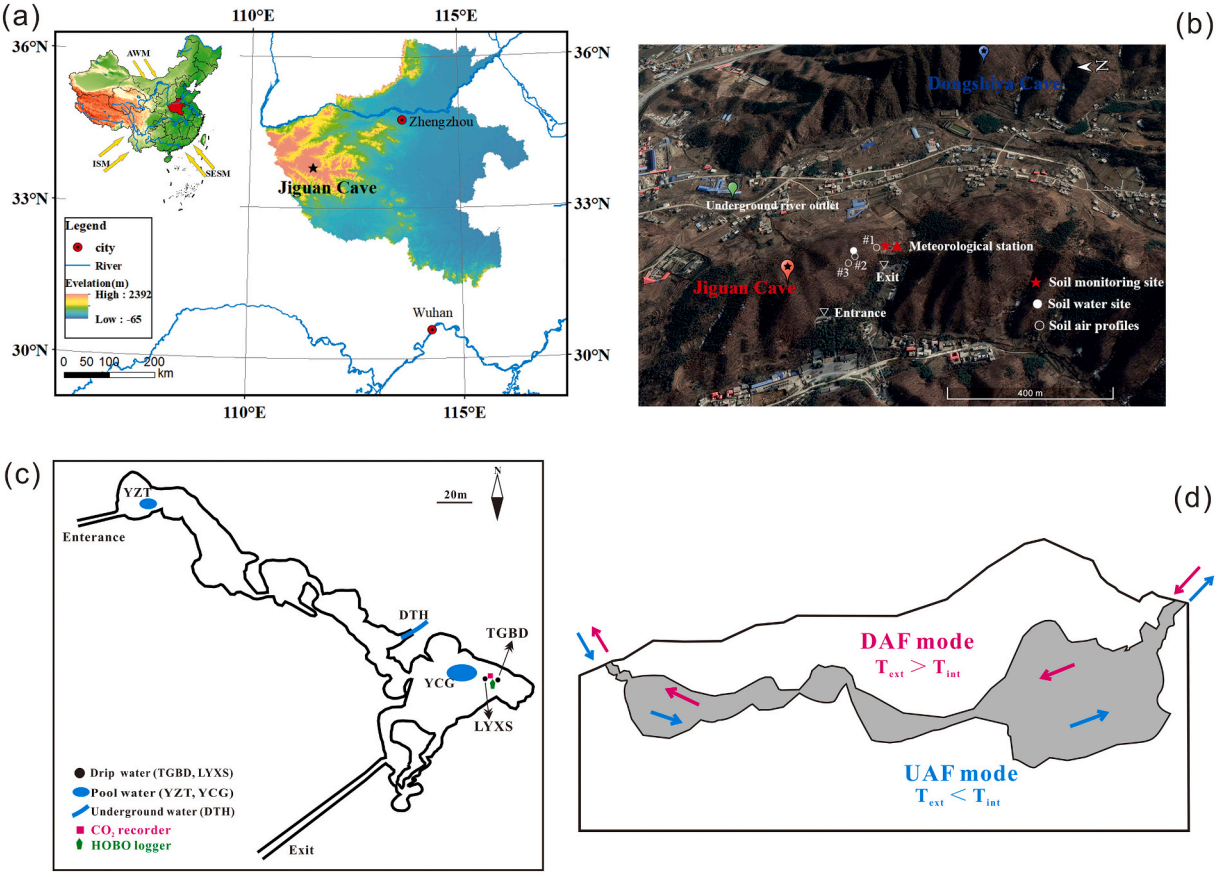

Fig. 1. (a) Locations of the study area and Jiguan cave (black star). Yellow arrows indicate Asian Winter Monsoon (AWM), Indian Summer Monsoon (ISM) and Southeast Summer Monsoon (SESM), respectively. ASTER DEM 30 m is used for elevation data. (b) Monitoring sites outside of the cave (base map obtained from Google Earth). (c) Monitoring sites inside the cave. YZT (Yu Zhu Tan) and YCG (Yao Chi Gong) are pools, LYXS (Li Yu Xi Shui) and TGBD (Tian Gong Bing Deng) are drips, DTH (Dong Tian He) is an underground river in the cave. Monitoring devices are placed next to the drip sites in the largest chamber. HOBO logger (green polygonal) is used for recording the temperature and humidity of the cave, cave pCO_2 is recorded by the CO_2 monitoring device (pink rectangular). The drip logger was placed at the drip site LYXS. (d) Sketch of the vertical profile of the cave and two ventilation modes with airflow direction. Blue arrows indicate downward airflow (DAF) mode with external air temperature (T_{ext}) warmer than internal cave-air temperature (T_{int}), and pink arrows show the upward airflow (UAF) mode with $T_{int} > T_{ext}$.

the bottom of the bottle and left above ground to allow extraction without removal of the soil. The end of the silicone tube was sealed before and after sampling to avoid contamination by atmosphere or dust. All components used for collecting soil water were ultrasonically cleaned with deionized water and dried after soaking in 50 % hydrochloric acid for 24 h (Chen and Li, 2018). The polypropylene bottles used to collect the water samples were rinsed in 1:1 HCl, then washed with deionized water and dried before sampling. Filtered soil water was added to the sample bottles by using the prewashed 0.22 μm Millipore nitrocellulose filters. To avoid isotopic fractionation caused by microorganisms, 0.2 ml of saturated $HgCl_2$ solution was added to the dissolved inorganic carbon (DIC) samples (Li et al., 2011). Soil-water samples were taken monthly from September 2019 to December 2021. Some sample data are missing due to low water storage in the soil layer during the dry season or the interruption of sampling caused by natural factors.

According to the different vegetation and soil conditions above the cave, three sites (numbered #1, #2, and #3, Fig. 1b) were excavated to collect soil-air CO_2 samples at depths of 30–40 cm in the soil profile at altitudes of 900–920 m. The soil-air CO_2 collection device (Fig. S1c) consists of a silicone tube connected to a 50 cm long, 3 cm diameter air collection tube with drilled holes on the surface that ensure full contact with the surrounding soil. The other side of the silicone tube sticks out of the ground and is sealed by a plastic plug to avoid the effect of the atmosphere. Composite polyethylene foil bags were used to store air samples. A gas pump was used to remove residual gas from the bag before collecting gas samples to avoid contaminating samples. To reduce the influence of human respiration on the cave air, the sampler held their breath while collecting air samples inside the cave and kept a distance of 2–3 m from the air inlet. Approximately 1 L each of soil and cave air near the drip site (LYXS) was extracted monthly and stored in a sealed container during 2021.

Five sites were set up inside the cave to collect cave water including two drip sites (LYXS and TGBD), an underground river (DTH), and two pool water sites (YZT and YCG). The drip water was pre-collected by a pre-cleaned plate (not acid-washed) left for 1–3 h before sampling. All cave water samples were collected by the same method as soil water and sampled monthly from April 2019 to 2021, intensive sampling was conducted every 2–6 h during rainfall events in July 2021. All samples were sealed and quickly transported back to the laboratory and refrigerated at 4 °C for approximately 2– 4 weeks prior to stable-isotope analysis.

3.2. Data collection from high-resolution monitoring instruments

Table 1 provides the instruments used for monitoring. A VantagePro field weather station was installed above the cave to automatically monitor temperature and precipitation data with an accuracy of 0.1 °C and 0.01 mm, respectively, at 15-minute intervals. EOS GP CO_2 concentration sensor (Eosense, Canada), AV-EC5 soil moisture sensor and AV-10T soil temperature sensor were installed near the weather station in May 2019 to monitor soil CO_2 concentration, temperature, and humidity overlying the cave and collect data with RR1016 data collector, respectively. The range of the soil CO_2 concentration sensor is 0 to 20,000 $mg{\cdot}L^{-1}$ with ±1 % accuracy; the range of the soil temperature sensor is −40 to +140 °C with ±0.1 °C accuracy; the range of the soil humidity sensor is 0 to 100 % with ±0.1 % accuracy. All sensors above gave high-precision continuous monitoring at 15-minute intervals.

The largest chamber with drip water sites (LYXS and TGBD) was chosen to monitor the microclimatic parameters inside the cave (Fig. 1c). HOBO U23 series temperature and humidity loggers were placed next to drip sites to record temperature and humidity values at 1-hour intervals from 2018. The pCO_2 inside and outside the cave has been measured at two-month intervals starting in 2017 and at one-month intervals starting in April 2019 using a TESTO 535 infrared CO_2 tester with a range of 0 to 9999 ppm and testing precision better than 2 %. Cave pCO_2 was monitored at 30-minute intervals by using a GSS1 CO_2 concentration sensor (range of 400–10,000 ppm, precision ±30 ppm) from June 2021 until now. The drip rate was recorded at 1-minute intervals at the drip site LYXS (Fig. 1c) using a Stalagmate plus Mk 3 during heavy rainfall events in July 2021. Note that some data were discontinuous due to equipment failure and the Coronavirus epidemic in 2020.

Table 1
Summary of the instruments used for monitoring.

Instruments	Observation variables	Accuracy	Recording interval	Operation period
DAVIS Vantage Pro2 weather station (Davis Inc., US)	T and P	0.1 °C; 0.01 mm	15 min	Apr 2019–Dec 2021
EOS GP CO_2 concentration sensor (Eosense, Canada)	Soil pCO_2	1 %	15 min	May 2019–Dec 2021
AV-10T soil temperature sensor (Eosense, Canada)	Soil T	0.1 °C	15 min	May 2019–Dec 2021
AVEC5 soil moisture sensor (Eosense, Canada)	Soil RH	0.1 %	15 min	May 2019–Dec 2021
HOBO U23-001A (Onset, US)	Cave T and RH	0.2 °C; 2.5 %	1 h	Feb 2018–Dec 2021
GSS1 gas CO_2 concentration sensor (Goodsellsystems, UK)	Cave pCO_2	30 ppm	30 min	June 2021–Dec 2021
TESTO 535 infrared CO_2 tester (Testo, Germany)	pCO_2 (in) outside of cave	2 %	2/1 month	Feb 2017–Dec 2021
Stalagmate plus Mk 3 (Diptych, UK)	Drip rate	5 drops/s	1 min	19th July–28th July 2021

Where T, P, and RH are air temperature, precipitation, and relative humidity, respectively.

3.3. Carbon-isotope analysis

All $\delta^{13}C_{DIC}$ analyses were conducted in the Isotope Laboratory of the Institute of Karst Geology, Chinese Academy of Geological Sciences using a MAT 253 isotope ratio mass spectrometer coupled to a Gas Bench II, with analytical precision better than 0.2 ‰ (1σ). Soil- and cave-air $\delta^{13}C$ samples were measured at the State Key Laboratory of Environmental Geochemistry, Institute of Geochemistry, Chinese Academy of Sciences, using a MAT 252 gas isotope ratio mass spectrometer, with analytical precision better than 0.2 ‰ (1σ). All carbon-isotope results are reported relative to Vienna Pee Dee Belemnite (VPDB) standard.

3.4. Calculations/analyses

Correlation analyses between visitors and cave pCO_2 were calculated by Pearson correlation coefficient and performed using the IBM SPSS Statistics.

4. Results

4.1. CO_2 concentration of soil and cave air

Soil-air CO_2 data from above Jiguan Cave are shown in Fig. 2. Soil CO_2 concentration exhibits a common seasonal pattern with soil temperature, which tracks local air temperature and precipitation. Soil CO_2 concentrations are highest (>5000 ppm) during the wet summer months and decrease sharply after the onset of autumn to reach minimum values (<900 ppm) in the winter. The highest soil-air CO_2 value in three years was recorded in September 2021, corresponding to an extreme rainfall

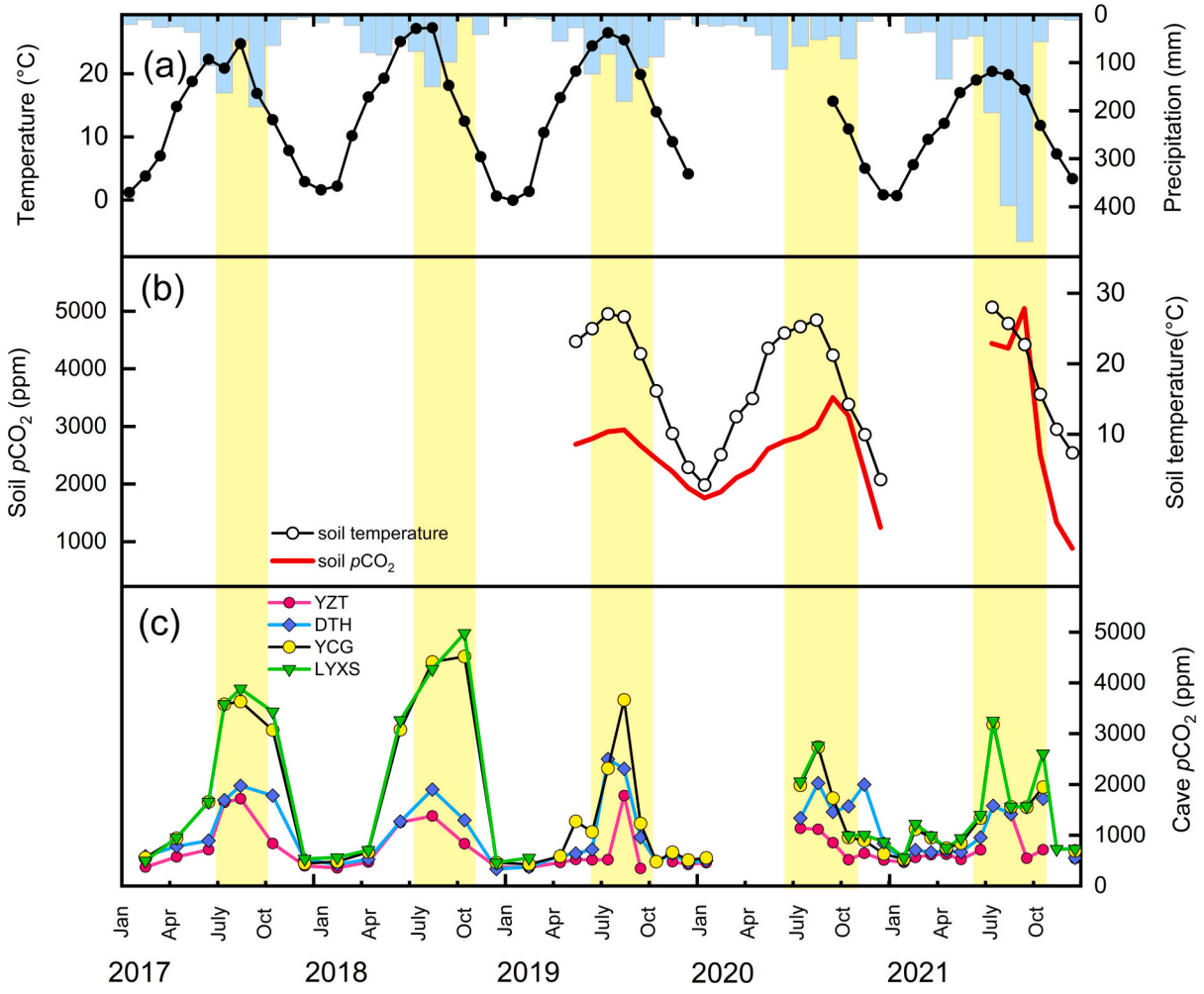

Fig. 2. Variation of soil air pCO_2 (2019–2021) and cave air pCO_2 (2017–2021). (a) The variety of temperature and precipitation. (b) Soil temperature and CO_2 concentration overlying the cave. (c) Cave air pCO_2 in four monitoring sites. Yellow shades represent rainy season precipitation and CO_2 peaks of cave air and soil air.

event in which 472 mm fell during the month. The lowest value occurred in December of the same year, with a seasonal amplification of up to 4162 ppm (Fig. 2b).

The concentration of cave-air CO_2 exhibited the same seasonal variation as soil CO_2 but with lower absolute values. Cave-air CO_2 concentrations are highest during summer months with mean value of 2153 ppm, and CO_2 values near the drip site as high as 4980 ppm were recorded. In winter, CO_2 levels in cave are generally lower but more stable, with a mean value close to that of atmospheric CO_2 (377 ppm). Mean values of CO_2 concentrations in the four monitoring sites were 727 ppm (YZT), 1071 ppm (DTH), 1553 ppm (YCG), and 1725 ppm (LYXS). Drip site LYXS and its nearby pool water site YCG in the same chamber showed similar trends and magnitudes of pCO_2, and both were much higher than at DTH and YZT (Fig. 2c).

4.2. $\delta^{13}C$ of CO_2 in soil and cave air

During the 2021 monitoring period, the $\delta^{13}C_{CO2}$ of both soil and cave air exhibited a significant and common seasonal signal, with lower values in summer/autumn and higher values in winter (Fig. 3a). The trends are consistent with those of local temperature, precipitation, and pCO_2 of soil and cave air. Measurements of $\delta^{13}C_{CO2}$ at our three soil sites (#1, #2, and #3) ranged from −15.2 ‰ to −22.2 ‰, −16.3 ‰ to −24.7 ‰, and −17.1 ‰ to −24.3 ‰, with mean values of −18.5 ‰, −20.8 ‰, and −21.1 ‰, respectively. Cave-air $\delta^{13}C_{CO2}$ ranged from −14.4 ‰ to −22.7 ‰ with a mean value of −18.6 ‰. The highest values of $\delta^{13}C_{CO2}$ in cave and soil air occurred in January and February, while the lowest values occurred in October and September. The mean value and range of cave-air $\delta^{13}C_{CO2}$ were close to those of soil-air site #1, while sites #2 and #3 were systematically lower (especially soil site #3) by up to 3 ‰, which we suggest may be related to soil moisture and/or the vegetation cover.

4.3. $\delta^{13}C$ of CO_2 in cave air at different stages of tourist activity

Three stages of tourist activity were divided according to visitor amounts from July 17 to August 4, 2021 and correspond to periods with or without human activity. During each stage, we measured the CO_2 concentration and cave-air $\delta^{13}C$ (Table 2). Cave-air pCO_2 levels at Stage 1 and 3 are generally more than twice that of Stage 2, when tourists were absent, and the sharpness of the transition between the first two stages is also reflected in a 2.4 ‰ rise in $\delta^{13}C$. The concentration of CO_2 remained stable but low during Stage 2, after which it rose by ~1400 ppm during Stage 3. Unfortunately, the $\delta^{13}C$ of cave air is not available from this stage.

4.4. $\delta^{13}C$ variation in karst system at the different rainfall stages

To investigate the characteristics of carbon-isotope transport and vertical variation at the scale of a single intense precipitation event, higher resolution monitoring was conducted in Jiguan Cave from July 17 to July 25, 2021 during a week-long episode of highly elevated

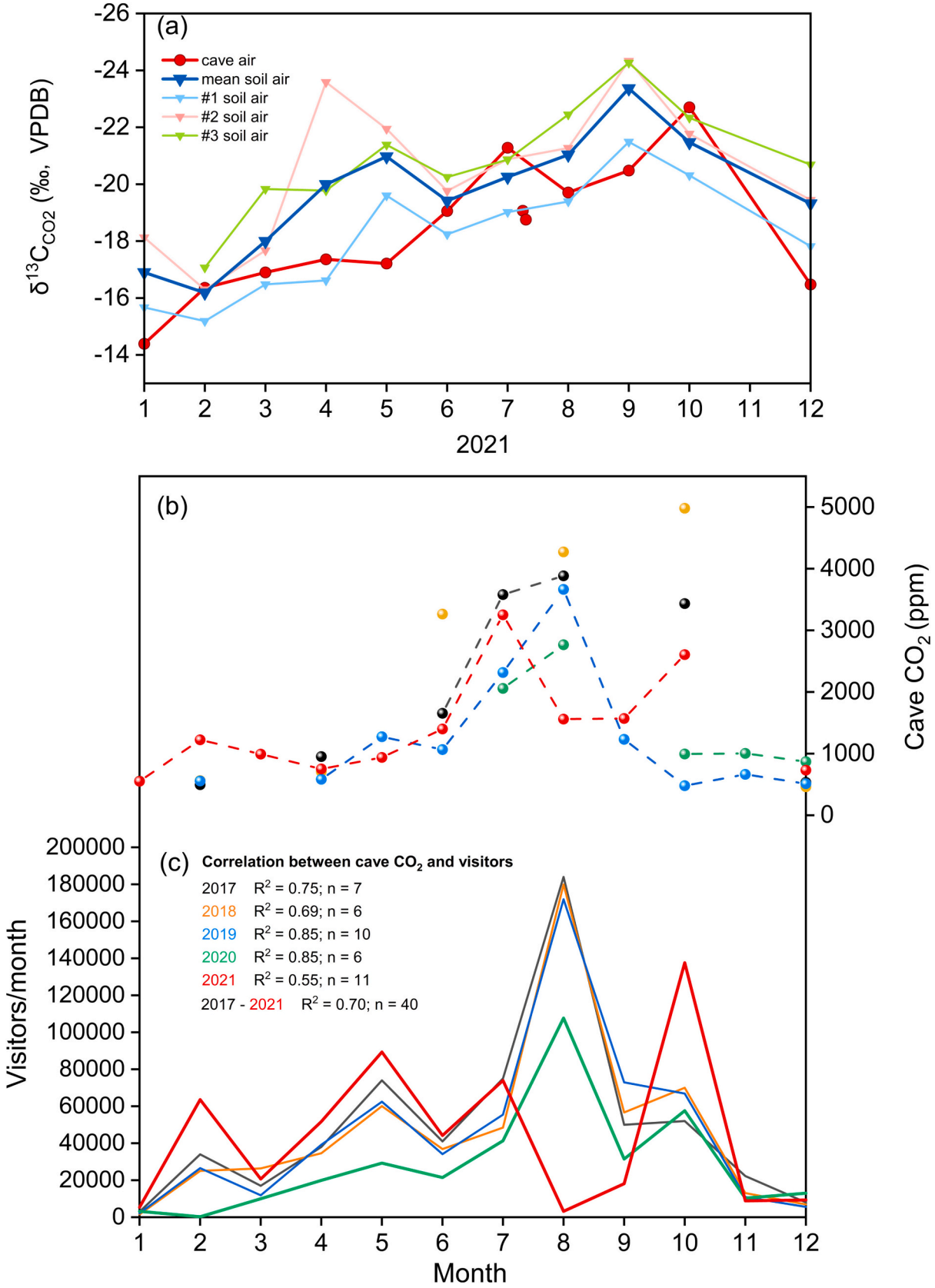

Fig. 3. (a) Variation of soil air $\delta^{13}C_{CO2}$ and cave air $\delta^{13}C_{CO2}$ during 2021. The dark blue line indicates mean values of $\delta^{13}C_{CO2}$ in soil air from three sites. Two red circles indicated cave air $\delta^{13}C_{CO2}$ measured during the heavy rainfall event on July 23 and July 24, 2021. (b) Monthly cave CO_2 in the main chamber from 2017 to 2021. (c) Monthly visitor amounts and their correlation with cave CO_2 from 2017 to 2021.

Table 2
Stage division based on tourists and variation of pCO_2 and $\delta^{13}C$ in cave air.

Stage	Date	Tourist amounts	pCO_2 (ppm)	$\delta^{13}C_{CO2}$ (‰, VPDB)
1	7/17 0:00– 7/21 23:30	6694	1267–4074	−21.3
2	7/22 0:00– 7/25 23:30	0	1166–1449	−19.1 ~ −18.8
3	7/26 0:00– 8/4 23:30	8433	1226–2852	–

– indicates missing data.

rainfall. The event was divided into three stages (Table 3), according to the intensity of precipitation. The heaviest rainfall occurred in Stage 3 at 18:00 on 21st July, with precipitation reaching 20 mm in 15 min.

Influenced by the intensity of precipitation and sampling interval, only one soil-water sample was taken in each stage. Soil-water $\delta^{13}C_{DIC}$ decreased progressively through the event by 2.8 ‰ (Table 3). The value of cave-air $\delta^{13}C_{CO2}$ was −21.3 ‰ during Stage 1 and −18.9 ‰ during Stage 2, with an amplitude of 2.4 ‰. Dripwater $\delta^{13}C_{DIC}$ varied by only 1.4 ‰ between stages, but measurable differences were observed. The value was −13.4 ‰ in Stage 1, slightly lower than the Stage 2 mean value of −12.8 ‰ (ranging from −11.3 ‰ to −13.6 ‰) but comparable to the Stage 3 value (mean −13.2 ‰). The $\delta^{13}C_{DIC}$ value of drip water reached the lowest value of −14.0 ‰ in the last sampling on July 28. $\delta^{13}C_{DIC}$ values of the underground river fluctuated in the range of −18.7 ‰ to −10.3 ‰, and the underground river outlet fluctuated from −21.5 ‰ to −9.9 ‰ (Table S2). The trend of $\delta^{13}C_{DIC}$ in both monitoring sites showed a "V"-shaped variation and a significant negative deviation in the second stage and a significant positive deviation in the last stage (Table 3).

5. Discussion

5.1. Carbon source analysis of cave CO_2

Cave-air CO_2 generally originates from (1) external atmospheric CO_2; (2) CO_2 produced by biological processes in the overlying soil (including plant root respiration and decomposition of organic matter by microorganisms); (3) decomposition of organic matter and respiration of microorganisms in caves; (4) deep geological sources (release of CO_2 by geothermal activity through faults and fissures) (Spötl et al., 2005; Baldini et al., 2008; Breecker et al., 2012; Pu et al., 2017; Mattey et al., 2021). The deep geothermal source is not considered in this study, because there are no mapped faults in Jiguan Cave.

5.1.1. Estimation of $\delta^{13}C$ of the end-member

The close correlation of soil- and cave-air CO_2 concentrations at Jiguan Cave, with high summer/autumn and low winter values, is consistent with a mechanistic link (Fig. 2). Mean values of cave-air $\delta^{13}C_{CO2}$ during summer are within 1.3 ‰ of the mean of overlying soil air (Table 4), suggesting that the seasonal signal of cave-air $\delta^{13}C$ may have been inherited from soil CO_2 through vertical transport. However, the high variability of $\delta^{13}C$ and higher winter values could reflect seasonal ventilation of the cave, driving the mixing between soil-respired and external atmosphere. In fact, the range of $\delta^{13}C$ in Jiguan Cave (8.3 ‰) is similar to that observed in Obir Cave, Blue Spring Cave and St. Michaels Cave (9 ‰, 10 ‰ and 13 ‰, respectively), where seasonal trends in $\delta^{13}C_{CO2}$ and pCO_2 are attributed to cold-season ventilation of the cave atmosphere. The summer/winter contrast in Jiguan Cave CO_2 (335–4980 ppm) is comparable to caves with significant seasonal ventilation, such as Obir Cave (~400–1500 ppm; Spötl et al., 2005), Crag Cave (~1100–8500 ppm; Baldini et al., 2008), Bunker Cave (~580–1200 ppm; Riechelmann et al., 2011), St. Michaels Cave (~600–8000 ppm; Mattey et al., 2016), Yangkou Cave (~200–6800 ppm; Li et al., 2018), and Blue Spring Cave (~400–1600 ppm; Druhan et al., 2021). Therefore, we suggest that the observed seasonal signal in cave CO_2 and $\delta^{13}C_{CO2}$ results from the interplay between soil dynamics and cold-season ventilation.

Table 4
$\delta^{13}C_{CO2}$ values of cave air and soil air from three sites during 2021.

Date	Cave air $\delta^{13}C$ (‰)	Soil air mean $\delta^{13}C$ (‰)	#1 $\delta^{13}C$ (‰)	#2 $\delta^{13}C$ (‰)	#3 $\delta^{13}C$ (‰)
2021/1/28	−14.4	−16.9	−15.7	−18.1	
2021/2/19	−16.4	−16.2	−15.2	−16.3	−17.1
2021/3/21	−16.9	−18.0	−16.5	−17.7	−19.8
2021/4/19	−17.4	−20.0	−16.6	−23.6	−19.8
2021/5/17	−17.2	−21.0	−19.6	−21.9	−21.4
2021/6/23	−19.1	−19.4	−18.2	−19.8	−20.3
2021/7/17	−21.3	−20.3	−19.0	−20.9	−20.9
2021/8/20	−19.7	−21.0	−19.4	−21.3	−22.4
2021/9/19	−20.5	−23.4	−21.5	−24.3	−24.3
2021/10/20	−22.7	−21.5	−20.3	−21.8	−22.3
2021/12/20	−16.5	−19.3	−17.8	−19.4	−20.7
Mean value in summer	−20.0	−20.2	−18.9	−20.6	−21.2
Mean value in winter	−15.7	−17.5	−16.2	−18.0	−18.9

Values of soil air $\delta^{13}C_{CO2}$ calculated by the average of three soil air sites #1, #2 and #3.

To test this hypothesis, we employ a Keeling plot end-member model to consider the processes of CO_2 production and diffusion in soil and epikarst zone (Nickerson and Risk, 2006). The pCO_2 of external (surface) atmosphere, soil air, and cave air, along with their $\delta^{13}C$ compositions, are shown in Fig. 4. From the Keeling plot results, all points are plotted on the left rather than strictly conformed to the line defining mixing between atmosphere and soil respired CO_2, which is consistent with observations from more than five caves (Druhan et al., 2021; Mattey et al., 2021; Kost et al., 2023). The respired member has an isotopic signature of −23.5‰, given by the intercepts of the black line on the y-axis (Fig. 3), which is higher than the $\delta^{13}C$ of respired soil CO_2 in soils dominated by C3 vegetation (range of −25‰ to −27.7‰; Cerling et al., 1991; Mattey et al., 2016, 2021). This is likely explained by the contribution of C4 plants with heavier isotopic components in the sampling soil site #1 (Fig. 3a). The data collected from this site yielded a mean soil CO_2 $\delta^{13}C$ value of −18.9 ‰ in summer (Table 4), which is comparable to the theory that 4.4 ‰ enrichment of $\delta^{13}C$ for soil CO_2 relative to soil-respired CO_2 (Cerling et al., 1991). Therefore, soil respired CO_2 might play a critical role in the contribution to cave air CO_2. Cave air CO_2 in winter months contains an isotopic composition of up to 6.9 ‰ higher than in summer (Fig. 4), which may be provided by atmospheric CO_2. Therefore, we infer that cave-air CO_2 oscillates within a mixing model comprised of two end members: 1) ^{13}C-depleted CO_2 originating from the overlying soil, and 2) the influx of external atmosphere with heavier isotopic compositions. The direct contribution of

Table 3
Precipitation, drip rate, and mean values of $\delta^{13}C_{DIC}$ in the vertical karst profile during heavy rainfall event.

Stage	Precipitation (mm)	Soil water $\delta^{13}C$ (‰)	Drip rate (drop/min)	Drip water mean $\delta^{13}C$ (‰)	Underground river mean $\delta^{13}C$ (‰)	Outlet mean $\delta^{13}C$ (‰)	Sample number
1	7.1	−13.2	84	−13.4	−10.3	−11.9	4
2	43.6	−13.9	78	−12.8	−16.6	−19.7	19
3	57.1	−16.0	153	−13.2	−10.4	−15.2	27

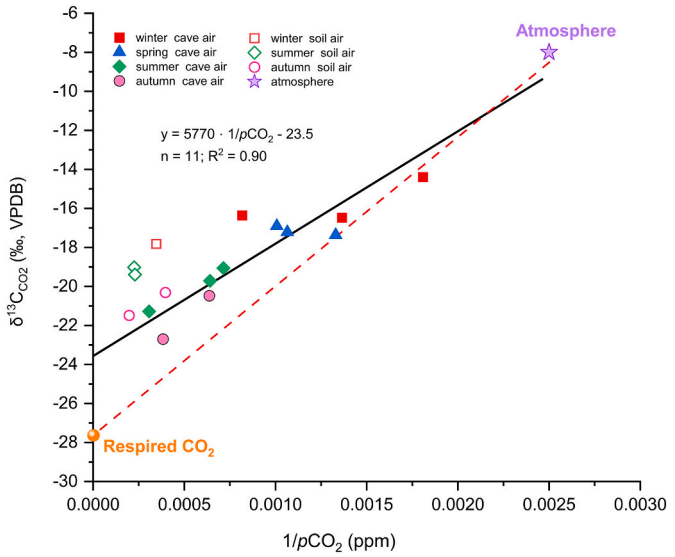

Fig. 4. Keeling plot of 1/(CO_2 concentration) versus isotopic composition of CO_2 in the atmosphere, cave, and soil air during 2021. The carbon isotope composition of cave air and soil air is shown by solid and open symbols, respectively. The black line is regressed by cave air measurements. The theoretical mixing line (thin red line) indicates a mixture between the two end-members of soil respired CO_2 (orange circle, $\delta^{13}C = -27.7$ ‰; Cerling et al., 1991) and the atmosphere (purple star, $\delta^{13}C = -8$ ‰ with $CO_2 = 400$ ppm), respectively (Druhan et al., 2021). Note that the relevant soil data are from soil site #1, which is the only site where soil pCO_2 was measured.

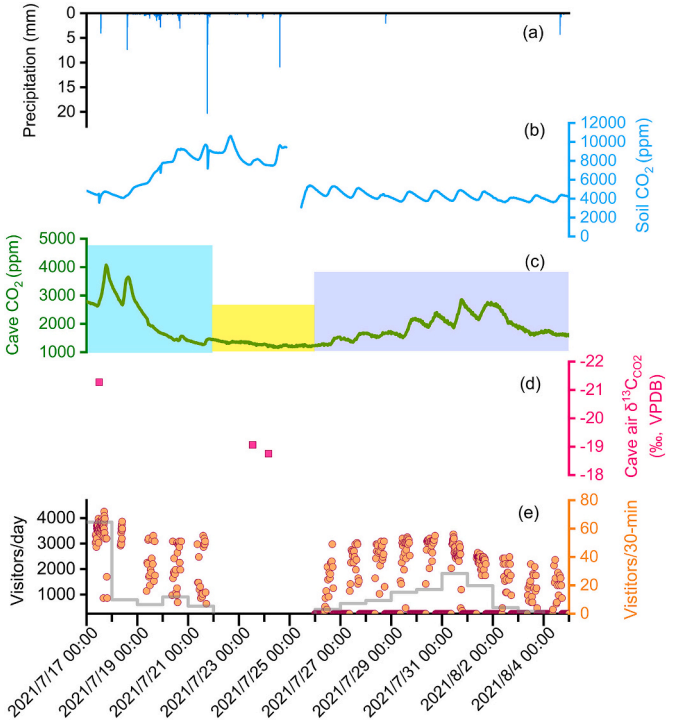

Fig. 5. Daily visitor amounts and cave-air pCO_2 in Jiguan Cave from July 17 to August 4, 2021. (a) Precipitation recorded at 15-minute intervals at the meteorological station above the cave. (b) Overlying soil pCO_2. (c) Cave pCO_2 recorded at 30-minute intervals. Blue, yellow, and purple shading denote three stages, respectively, based on the level of tourist activity (tourists – no tourists – tourists). (d) Cave-air $\delta^{13}C_{CO2}$ measured during visitors and no-visitor stages. (e) Daily visitors (gray line) and tourist amounts within 30-minute intervals (orange dots).

soil CO_2, which peaks in autumn, is exemplified by the overlap of cave and soil $\delta^{13}C_{CO2}$ during the warm season. Conversely, the lowest cave CO_2 and the highest $\delta^{13}C_{CO2}$ values occur mainly in winter and spring, approximately halfway between end-member compositions of soil-respired and atmospheric CO_2, indicating that cave-air $\delta^{13}C_{CO2}$ is strongly influenced by ventilation during the cold (dry) season.

Other potential sources of CO_2 in the cave include degassing from CO_2-rich groundwater (Breecker et al., 2012). Considering a 9 ‰ fractionation between water and gas (Zhang et al., 1995), the signature of CO_2 from degassing drip water would follow the seasonal cycle of drip water $\delta^{13}C$ with low amplitude. Enhanced (reduced) drip rates during summer (winter) could explain the accumulation of ^{13}C-depleted (-enriched) CO_2 during the monsoon (dry) season. Due to the vertical transport of soil CO_2 through percolating water as it flows along fractures in the epikarst zone and eventually enters the cave to form drip water (Banner et al., 2007; Li and Li, 2018), the aqueous CO_2 still derives largely from soil CO_2.

5.1.2. *The impact of tourism activities on the cave air composition*

Human respiration associated with cave tourism constitutes a potential source of cave CO_2 that can increase cave pCO_2 by an order of magnitude (Baker and Genty, 1998; Faimon et al., 2006; Lang et al., 2015; Liñán et al., 2023). On July 22, 2021, record-breaking rainfall in the Henan Province, China (Nie and Sun, 2022) led to a temporary closure of Jiguan Cave from July 22–25 (Stage 2), providing an opportunity to study short-term impacts of tourism on the cave environment. The complete absence of tourists during Stage 2 was coincident with a ~70 % decrease in cave pCO_2 and a 2.5 ‰ increase in cave-air $\delta^{13}C$ (Table 2). After the reopening of Jiguan Cave to tourists on July 26, cave pCO_2 steadily recovered within 7 days to ~3000 ppm (Fig. 5c), comparable to the pre-closure concentration. We attribute this 2000–3000 ppm fall and rise in pCO_2 over several days primarily to contributions from human respiration. Moreover, the average $\delta^{13}C_{CO2}$ value of human respiration is about −20 ‰ ~ −21 ‰ (Schoeller et al., 1980; Breecker et al., 2012), which is consistent with the $\delta^{13}C$ value of cave air CO_2 (−21.28 ‰) measured during Stage 1, indicating that CO_2 from human respiration could be the main contributor to cave CO_2 during the normal condition with tourism activity.

In the exceptional situation of the cave closure during Stage 2 (no tourists), the decreased cave pCO_2 reflected the disappearance of the anthropogenic CO_2 source (Fig. 5c), with the isotopic signal increases to the isotopic composition of soil CO_2 in July (Fig. 3a). Similar situation repeated in August 2021, the $\delta^{13}C$ of cave air was close to the isotopic signal of soil air (Fig. 3a and c) when visitors decreased 53–56 times the same month between 2017 and 2019 (Fig. 3a and c) due to the pandemic policy constraints. It suggested that soil CO_2 was the principal source of the cave CO_2 when the anthropogenic CO_2 source was removed.

Nevertheless, soil CO_2 maintained a continuous and smooth fluctuation during Stage 3 (Fig. 5b), when cave air CO_2 gradually increased under the influence of human activity, implying that the contribution of soil CO_2 to cave air was masked by human respiration. A significant decrease in cave-air $\delta^{13}C_{CO2}$ was observed in July and October in 2021, corresponding to two large peaks in tourist amounts (Fig. 3a). Along with the observation that cave-air values became even lower than the soil air following spikes in tourists, we conclude that contributions from human activity are a plausible short-term influence on cave pCO_2 and $\delta^{13}C_{CO2}$. In addition, the strong correlation between monthly cave CO_2 and visitors over seasonal scales from 2017 to 2021 further suggests that the effect of human respiration contribution cannot be neglected (Fig. 3b and c) although soil CO_2 was regarded as the dominant source of cave CO_2 in summer season has been proposed in Section 5.1.1. However, it is usually a challenge to strictly discriminate between the two sources of soil air and human respiration because of their similar trend and isotopic compositions. We conclude that the enriched-CO_2 isotopic signal of cave air in summer is attributed to the mixture of soil air and anthropogenic

respiration.

Overall, the available data suggest three principal sources of CO_2 in Jiguan Cave on a seasonal timescale: 1) high soil CO_2 produced by the warm and rainy conditions of the summer monsoon; and 2) atmospheric CO_2 introduced by winter ventilation; and 3) superimposed human respiration.

5.2. Primary controls on carbon transport in the soil-cave system

5.2.1. Soil CO_2

Overlying the roof of Jiguan Cave is a dense cover of predominantly C3 vegetation ($\delta^{13}C = -26.0 \pm 1.2$ ‰; Li et al., 2021). The summer increase in local temperature and precipitation leads to enhanced microbial activity in the soil, which intensifies the decomposition of organic matter and respiration of plant roots, resulting in a substantial increase in soil pCO_2 (Fig. 2b) and up to an 8 ‰ decrease in soil-air $\delta^{13}C_{CO2}$ (Fig. 6b). Monsoonal rains absorb high volumes of soil CO_2 and carry the ^{13}C-depleted bicarbonate pool downward through bedrock conduits and fissures, resulting in both higher accumulation of CO_2 in the cave and lower $\delta^{13}C_{CO2}$ values of cave air. When temperature and precipitation are lower in winter, reduced soil activity and plant root respiration lead to a decrease in soil CO_2 and higher soil-air $\delta^{13}C_{CO2}$. Diffusion and transport of soil CO_2 into the cave through the epikarst decreases, resulting in a concomitant increase in cave-air $\delta^{13}C_{CO2}$.

Although the mechanistic link of carbon-isotope transport within the karst system is well supported by geochemical and monitoring data, the response time of this process is difficult to constrain. The correlation between soil- and cave-air CO_2 shows no obvious lag in the respective seasonal cycles during 2021, but this absence is plausibly due to the influence of an exceptionally wet rainy season on aquifer residence time (Fig. 6a). Similarly, the strong negative $\delta^{13}C_{DIC}$ anomalies from the drip water and underground river (Fig. 6c) demonstrate that flushing of soil CO_2 through the karst system can occur rapidly in response to elevated precipitation. However, the contribution of conduit-flow degassing is likely small relative to the constant degassing from diffuse water flow, which exhibits a similar diminished seasonal amplitude with drip water $\delta^{13}C_{DIC}$. Future work should attempt to replicate the results from 2021, with a focus on vertical transport times of the $\delta^{13}C$ signal.

5.2.2. Ventilation effects

The density contrast between the cave and external atmosphere is determined by the temperature difference (ΔT), which can be used to indicate the direction of airflow and reveal ventilation status:

$$\Delta T = T_{ext} - T_{int}.$$

Negative ΔT values indicate that the temperature inside the cave is higher than the surface temperature, allowing the influx of atmosphere to the cave, and vice versa. Positive ΔT values occur from May to September, while negative ΔT values occur from October to April (Fig. S3).

Accordingly, two different ventilation states can be classified. During the winter half-year, negative ΔT values are associated with an unstable density gradient, in which the cave is actively ventilated as the density gradient drives colder, drier, and low-CO_2 atmosphere flow from the low entrances to the high entrance (UAF mode, Faimon et al., 2012) and dilute the cave air, reducing pCO_2 and increasing $\delta^{13}C_{CO2}$ in the cave. However, cave pCO_2 (average 670 ppm) were not completely reduced to the level of atmosphere (~410 ppm) that should be related to the contribution of visitors in winter. The reduction of cave-air CO_2 drives degassing of dissolved CO_2 from cave waters, which promotes calcite precipitation and leads to higher $\delta^{13}C_{DIC}$ in drip water (Fig. 6c). During the warm season under the conditions of the DAF mode, positive ΔT values are associated with a cold-air trap in the cave, resulting in the external air sucked into the cave though high entrance or the soil breathing spots and the outflow of cave air through the low entrance, promoting the advective flux of the soil-respired CO_2 deeper into the cave (Faimon et al., 2020) and accumulation of degassing CO_2 with low $\delta^{13}C$ values from the soil zone (Frisia et al., 2011; Dreybrodt et al., 2016). Calcite precipitation is inhibited by the CO_2-rich atmosphere and dripwater $\delta^{13}C_{DIC}$ is again reduced (Banner et al., 2007; Baldini et al., 2008; Oster et al., 2012). These processes are consistent with our observations from monitoring, as well as results from other caves, such as Desoto Cave (Lambert and Aharon, 2011), Nerja Cave (Liñán et al., 2020) and Xueyu Cave (Cao et al., 2021).

5.3. Spatiotemporal transport of carbon isotopes in the karst system

5.3.1. Carbon-isotope transport under varying rainfall intensity

The varying intensity of precipitation during the three stages (Table 3) had a significant influence on the spatial and temporal transport of carbon-isotope signals. The soil was relatively dry in early July (Stage 1) with low precipitation and strong evaporation (Fig. 7a). Due to the lack of effective precipitation, microbial activity was inhibited and plant root respiration rate relatively low, causing soil-water $\delta^{13}C_{DIC}$ to be higher (Fig. 7c). The main discharge of drip water derives from water stored in the aquifer, reflecting mixed climatic information (Lechleitner et al., 2018; Fohlmeister et al., 2020). The underground river and its outlet show high carbon-isotope characteristics simultaneously. In this stage, the mean $\delta^{13}C$ value of each component in the vertical karst profile exhibited a high anomaly due to the weak soil productivity under dry climatic conditions, with the exception of dripwater $\delta^{13}C_{DIC}$ (Table 3).

At the inception of low-intensity but continuous precipitation (Stage 2), the increase in soil moisture strengthened plant root respiration and microbial activity, resulting in more ^{12}C CO_2 gas being dissolved in the soil water, finally $\delta^{13}C$ values of soil water drop from −13.2 ‰ in Stage 1 to −13.9 ‰ in Stage 2. The old water stored in the karst fissure was pushed by the loading of infiltrating water and downward to the cave. However, the continuous rainfall did not reach the necessary threshold to infiltrate directly into the aquifer or mix sufficiently with stored water, which can be confirmed by the fact that the maximum precipitation recorded by the meteorological station was only 7.3 mm over 15 min, causing $\delta^{13}C_{DIC}$ of drip water to fluctuate and increase slightly from −13.4 ‰ to −12.8 ‰ (Fig. 7). Fractures above the underground river are more developed than drip water, however, and even the low intensity precipitation led to an abrupt drop in $\delta^{13}C$, perhaps associated with the repaid flushing of soil CO_2 into the system (Genty et al., 2003).

During Stage 3, the maximum precipitation rate (20 mm within 15 min) was recorded at the weather station. Because the soil layer overlying Jiguan Cave is thin, however, the residence time is very low for the throughflow, evidenced by the fact that only one soil water sample was collected. Consequently, soil-air CO_2 would not likely have time to dissolve fully into the infiltrating rainwater. Excess water in the soil pores would have hindered microbial activity and limited the plant root respiration, which eventually led to a depletion in soil CO_2 (Fig. 7b). This interpretation is also consistent with observed changes in soil CO_2 during a strong rainstorm event in Xueyu Cave (Cao et al., 2021). Based on previous studies of stalagmite $\delta^{13}C$, low retention of rainwater by soil can mitigate the solubility of soil CO_2 in percolating water, resulting in high $\delta^{13}C$ anomalies in stalagmites (Baker et al., 1997; Bar-Matthews et al., 2000; Kong et al., 2005). Thus in cases where thin soils overly karst areas, heavy rainfall events can partially bypass the soil zone into the fissures in the epikarst before equilibrium is reached (both in terms of pCO_2 and isotopic exchange), resulting in high carbon-isotope shifts in cave waters.

Compared with drip water, the underground river and outlet exhibit a more rapid response to short-duration intense precipitation. After the heavy rainfall, $\delta^{13}C$ of the underground river and outlet show significant up shifts of 6.2 ‰ and 4.5 ‰, respectively (Fig. 7). This disparity may be due to the different paths of fissures overlying the underground river. With the continuous outward transport, CO_2 degassing of the underground river favors an increase in $\delta^{13}C$ at its outlet.

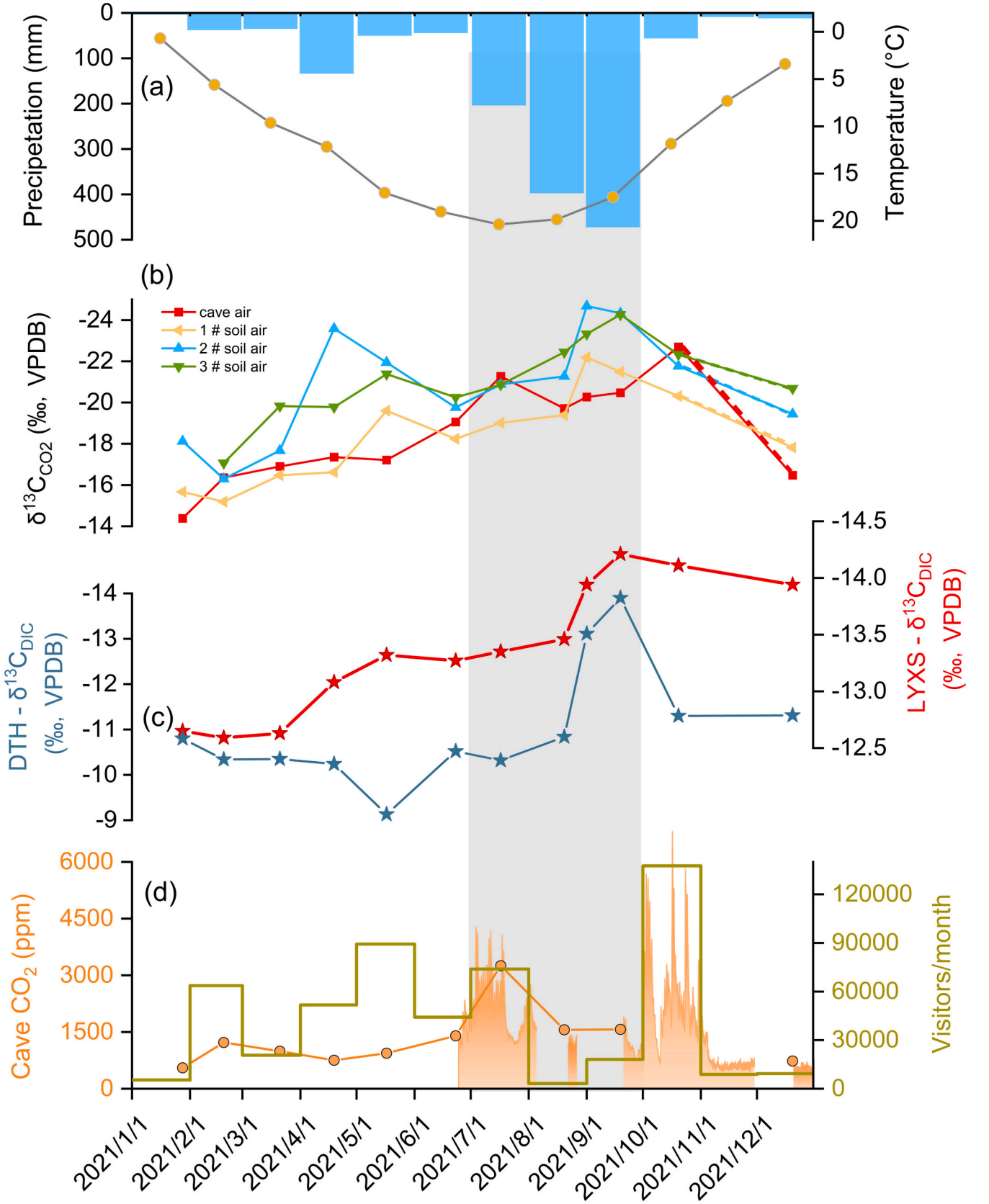

Fig. 6. Variation of carbon isotopes and pCO_2 in the soil-cave system during 2021. The gray bar represents the wet season. (a) Local monthly mean temperature and precipitation. (b) Variation of soil-air and cave-air $\delta^{13}C_{CO2}$. Three soil-air sites (numbered #1, #2, and #3) were excavated at depths of 30–40 cm in different soil profiles at altitudes of 900–920 m. (c) Cave water $\delta^{13}C_{DIC}$ of drip water LYXS (red star line) and underground river DTH (blue star line). (d) Monthly visitors (dark yellow line) and cave pCO_2 (orange lines). The orange dot line and solid line with profile indicate monthly measured cave pCO_2 and high-resolution cave pCO_2 recorded at 30-minute intervals, respectively.

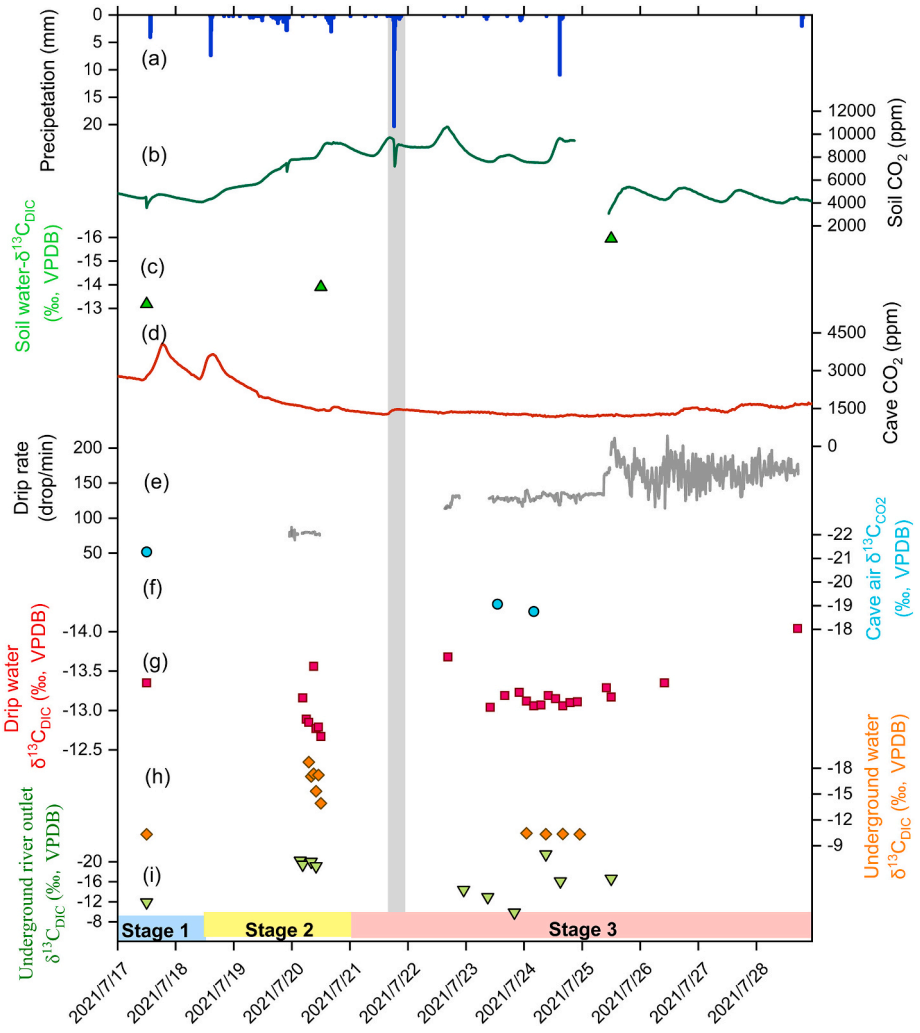

Fig. 7. Carbon-isotope measurements in the soil-cave system during a heavy rainfall event. Stage 1, Stage 2, and Stage 3 in the figure represent intervals with 1) no precipitation; 2) continuous precipitation, and 3) heavy precipitation. The gray shading denotes timing of the heavy precipitation event. (a) Precipitation recorded at 15-minute intervals at the meteorological station above the cave. (b) Overlying soil pCO_2. (c) Soil water $\delta^{13}C_{DIC}$ in three Stages (green triangles). (d) Cave pCO_2 recorded at 30-minute intervals. (e) Drip rate of LYXS. (f) Cave-air $\delta^{13}C_{CO2}$ measured in Stage 1 and Stage 3 (blue dots). (g) Drip water $\delta^{13}C_{DIC}$ (LYXS, red squares). (h) Underground river $\delta^{13}C_{DIC}$ (DTH, orange rhombus). (i) Underground river outlet $\delta^{13}C_{DIC}$ (light green triangles).

5.3.2. Spatial variation in carbon-isotope transport

Carbon isotopes show a stepwise increase in $\delta^{13}C$ along their transport path through the vertical karst profile from the plant-soil system to cave drip water, speleothem, and the underground river, while transport within the underground river to the outlet shows a decreasing trend in $\delta^{13}C$ (Fig. 8). Within our soil profiles, the $\delta^{13}C$ of soil organic matter (-16.7 ± 2.2 ‰) is higher than that of the overlying vegetation (-26.0 ± 1.2) by 9.3 ‰, which may be related to fractionation during microbial decomposition during the warm season (Li et al., 2021). The mean $\delta^{13}C_{DIC}$ of drip water is near that of soil water, indicating that contributions to the DIC pool from bedrock dissolution are minimal (Baker et al., 1997; Fairchild et al., 2006), so that the soil-$\delta^{13}C$ signal is largely preserved during transport within the fissure conduits of the karst system (Tooth and Fairchild, 2003). The $\delta^{13}C_{DIC}$ signal can increase further between drip water and speleothem calcite due to CO_2 degassing and PCP, both of which preferentially remove ^{12}C (Hendy, 1971; Luo and Wang, 2009; Fohlmeister et al., 2020). Regular monitoring of both values from 2009 to 2017 showed that such enrichment is up to ~5 ‰ and is generally strong during winter, when pCO_2 is lower (Li et al., 2021).

Underground river $\delta^{13}C_{DIC}$ is further modulated by variable contributions of bedrock carbonate to biogenic (soil) CO_2 through carbonate dissolution (Hendy, 1971; Fairchild et al., 2006). Compared with the diffuse transport feeding drip water, the pipeline fissures above the underground river are more developed and interconnected. As the $\delta^{13}C$ value of bedrock is higher than that of the soil source (Hendy, 1971), groundwater shows an enriched carbon-isotope signal. $\delta^{13}C$ of the underground river outlet decreases significantly (Fig. 8), which may be the result of picking up new biogenic CO_2 from the surrounding plants (Liu et al., 2008). However, the specific reasons need to be further discussed in future studies in the context of discharge variations in the underground river and its outlet.

6. Conclusions

In this study, we analyzed carbon-isotope compositions in multiple components of the karst system at Jiguan Cave in Funiu Mountains of central China to explore the characteristics of carbon sources and transport mechanisms, as well as the response of $\delta^{13}C$ to local climatic and environmental perturbations. Especially, the cave closure period provided an opportunity to study the variations of microclimate conditions and carbon sources without human activity. Cave-air pCO_2 and $\delta^{13}C_{CO2}$ varies synchronously with the overlying soil air with a seasonal amplitude, due to changes in hydrological conditions. High-resolution

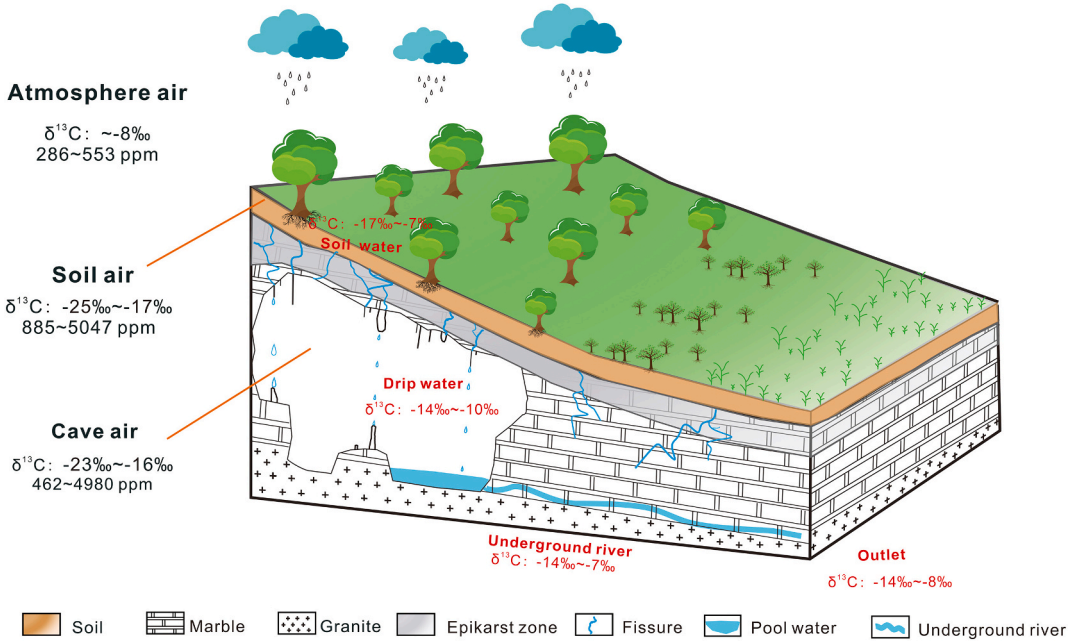

Fig. 8. A sketch of the vertical profile of the karst system in the study area and $\delta^{13}C$ values of different components. Values of $\delta^{13}C_{CO2}$ in the external atmosphere, soil-air, and cave-air obtained from 2021, $\delta^{13}C_{DIC}$ values of soil water, drip water, underground river, and the outlet river were integrated from monthly data between 2018 and 2021.

and multi-year monitoring results identified human respiration as a significant non-climatic factor that can substantially modify cave pCO_2 up to 3000 ppm and carbon-isotope composition, but this effect is superimposed on the seasonal soil-CO_2 signal. ^{13}C-enriched isotopic composition of cave air in summer can be attribute to the contributions from the external atmosphere through active ventilation (UAF mode) in winter. Although the $\delta^{13}C$ signal reflects complex vertical processes in the karst system, it can be utilized to interpret rainfall intensity and regional hydroclimate. In response to heavy rainfall events, excessive precipitation and rapid transit through the soil zone may lead to anomalously high values of $\delta^{13}C$ in the cave system, due to incomplete isotopic exchange with soil-respired CO_2. Due to the importance of CO_2 in the karst processes, more caution should be paid to evaluate the CO_2 sources and transport using monitoring results from anthropogenically affected caves in the karst system.

CRediT authorship contribution statement

Yidong Li: Writing – review & editing, Writing – original draft, Investigation, Formal analysis. **Yan Yang:** Writing – review & editing, Project administration, Funding acquisition, Conceptualization. **Xianguo Wang:** Resources. **Weijun Luo:** Resources. **Jingyao Zhao:** Writing – review & editing. **Zhe Sun:** Writing – review & editing. **Zhimao Ye:** Investigation, Data curation. **Xiaomin Chen:** Investigation, Data curation. **Xiao Shi:** Investigation, Data curation. **Yanzhi Xu:** Resources. **Jonathan L. Baker:** Writing – review & editing.

Declaration of competing interest

The authors declare that they have no known competing financial interests or personal relationships that could have appeared to influence the work reported in this paper.

Data availability

Data will be made available on request.

Acknowledgments

This research was supported by the National Natural Science Foundation of China (Nos 42277048, 41877450) to Y. Yang, and China Scholarship Council (202206990005) to Y. Li. We appreciate Yao Wu and Rui Zhang for helping to carry out the sampling work during the rainstorm. We also would like to thank the staffs of Jiguan Cave for their continual support over the years.

Appendix A. Supplementary data

Supplementary data to this article can be found online at https://doi.org/10.1016/j.scitotenv.2024.170507.

References

Atkinson, T.C., 1977. Carbon dioxide in the atmosphere of the unsaturated zone: an important control of groundwater hardness in limestones. J. Hydrol. 35, 111–123.
Baker, A., Genty, D., 1998. Environmental pressures on conserving cave speleothems: effects of changing surface land use and increased cave tourism. J. Environ. Manage. 53, 165–175.
Baker, A., Ito, E., Smart, P.L., McEwan, R.F., 1997. Elevated and variable values of ^{13}C in speleothems in a British cave system. Chem. Geol. 136, 263–270.
Baldini, J.U.L., Mcdermott, F., Hoffmann, D.L., Richards, D.A., Clipson, N., 2008. Very high-frequency and seasonal cave atmosphere pCO_2 variability: implications for stalagmite growth and oxygen isotope-based paleoclimate records. Earth Planet. Sci. Lett. 272, 118–129.
Banner, J.L., Guilfoyle, A., James, E.W., Stern, L.A., Musgrove, M., 2007. Seasonal variations in modern speleothem calcite growth in Central Texas, USA. J. Sediment. Res. 77, 615–622.
Bar-Matthews, M., Ayalon, A., Kaufman, A., 2000. Timing and hydrological conditions of Sapropel events in the Eastern Mediterranean, as evident from speleothems, Soreq cave, Israel. Chem. Geol. 169, 145–156.
Behzad, H.M., Arif, M., Duan, S., Kavousi, A., Cao, M., Liu, J., Jiang, Y., 2023. Seasonal variations in water uptake and transpiration for plants in a karst critical zone in China. Sci. Total Environ. 860, 160424.
Bergel, S.J., Carlson, P.E., Larson, T.E., Wood, C.T., Breecker, D.O., 2017. Constraining the subsoil carbon source to cave-air CO_2 and speleothem calcite in central Texas. Geochim. Cosmochim. Acta 217, 112–127.
Breecker, D.O., Payne, A.E., Quade, J., Banner, J.L., Ball, C.E., Meyer, K.W., Cowan, B.D., 2012. The sources and sinks of CO_2 in caves under mixed woodland and grassland vegetation. Geochim. Cosmochim. Acta 96, 230–246.
Breitenbach, S.F.M., Lechleitner, F.A., Meyer, H., Diengdoh, G., Mattey, D., Marwan, N., 2015. Cave ventilation and rainfall signals in dripwater in a monsoonal setting - a monitoring study from NE India. Chem. Geol. 402, 111–124.

Cao, M., Jiang, Y.J., Chen, Y., Fan, J., He, Q., 2020. Variations of soil CO_2 concentration and pCO_2 in a cave stream on different time scales in subtropical climatic regime. Catena 185, 104280.
Cao, M., Lei, J., He, Q., Zeng, Z., Lü, X., Jiang, Y.J., 2021. Rainfall-driven and hydrologically-controlled variations in cave CO_2 sources and dynamics: evidence from monitoring soil CO_2, stream flow and cave CO_2. J. Hydrol. 595, 126060.
Cerling, T.E., Solomon, D.K., Quade, J., Bowman, J.R., 1991. On the isotopic composition of carbon in soil carbon dioxide. Geochim. Cosmochim. Acta 55, 3403–3405.
Chen, C.J., Li, T.-Y., 2018. Geochemical characteristics of cave drip water respond to ENSO based on a 6-year monitoring work in Yangkou Cave, Southwest China. J. Hydrol. 561, 896–907.
Chen, X., Jiang, X., Wang, X., Zhao, J., Sun, Z., Li, Y., Ye, Z., Cai, J., Fu, X., Xu, Y., Yang, Y., 2023. New insights into potential effects of solar activity on the oxygen isotope composition of modern speleothems: observations from Jiguan Cave, central China II. J. Hydrol. 625, 130114.
Covington, M., 2016. The importance of advection for CO_2 dynamics in the karst critical zone: an approach from dimensional analysis. Caves Karst Across Time 113–127.
Dreybrodt, W., Hansen, M., Scholz, D., 2016. Processes affecting the stable isotope composition of calcite during precipitation on the surface of stalagmites: laboratory experiments investigating the isotope exchange between DIC in the solution layer on top of a speleothem and the CO_2 of the cave atmosphere. Geochim. Cosmochim. Acta 174, 247–262.
Druhan, J.L., Lawrence, C.R., Covey, A.K., Giannetta, M.G., Oster, J.L., 2021. A reactive transport approach to modeling cave seepage water chemistry I: carbon isotope transformations. Geochim. Cosmochim. Acta 311, 374–400.
Faimon, J., Štelcl, J., Sas, D., 2006. Anthropogenic CO_2-flux into cave atmosphere and its environmental impact: a case study in the císařská cave (Moravian karst, Czech republic). Sci. Total Environ. 369, 231–245.
Faimon, J., Troppová, D., Baldík, V., Novotný, R., 2012. Air circulation and its impact on microclimatic variables in the Císařská Cave (Moravian Karst, Czech Republic). Int. J. Climatol. 32, 599–623.
Faimon, J., Lang, M., Geršl, M., Sracek, O., 2020. The "breathing spots" in karst areas—the sites of advective exchange of gases between soils and adjacent underground cavities. Climatology 142, 85–101.
Fairchild, I.J., Smith, C.L., Baker, A., Fuller, L., Spötl, C., Mattey, D., McDermott, F., E.I. M.F., 2006. Modification and preservation of environmental signals in speleothems. Earth Sci. Rev. 75, 105–153.
Fairchild, I.J., Baker, A., Asrat, A., Domínguez-Villar, D., Gunn, J., Hartland, A., Lowe, D., 2012. Speleothem Science: From Process to Past Environments [M].
Fohlmeister, J., Scholz, D., Kromer, B., Mangini, A., 2011. Modelling carbon isotopes of carbonates in cave drip water. Geochim. Cosmochim. Acta 75, 5219–5228.
Fohlmeister, J., Voarintsoa, N.R.G., Lechleitner, F.A., Boyd, M., Brandtstätter, S., Jacobson, M.J., L. Oster, J., 2020. Main controls on the stable carbon isotope composition of speleothems. Geochim. Cosmochim. Acta 279, 67–87.
Frisia, S., Fairchild, I.J., Fohlmeister, J., Miorandi, R., Spötl, C., Borsato, A., 2011. Carbon mass-balance modelling and carbon isotope exchange processes in dynamic caves. Geochim. Cosmochim. Acta 75, 380–400.
Genty, D., Blamart, D., Ouahdi, R., Gilmour, M., Baker, A., Jouzel, J., Van-Exter, S., 2003. Precise dating of Dansgaard-Oeschger climate oscillations in western Europe from stalagmite data. Nature 421, 833–837.
Hendy, C.H., 1971. The isotopic geochemistry of speleothems-I. The calculation of the effects of different modes of formation on the isotopic composition of speleothems and their applicability as palaeoclimatic indicators. Geochim. Cosmochim. Acta 35, 801–824.
Kong, X., Wang, Y., Wu, J., Cheng, H., Edwards, L.R., Wang, X., 2005. Complex response and diagnosis of Nanjing Huludong stalagmite $\delta^{13}C$ to ice age climate. Sci. Sin. 35, 1047–1052.
Kost, O., González-Lemos, S., Rodríguez-Rodríguez, L., Sliwinski, J., Endres, L., Haghipour, N., Stoll, H., 2023. Relationship of seasonal variations in drip water $\delta^{13}C_{DIC}$, $\delta^{18}O$, and trace elements with surface and physical cave conditions of La Vallina cave, NW Spain. Hydrol. Earth Syst. Sci. 27, 2227–2255.
Kukuljan, L., Gabrovšek, F., Johnston, V.E., 2021. Low-calcium cave dripwaters in a high CO_2 environment: formation and development of corrosion cups in Postojna Cave, Slovenia. Water 13, 3184.
Lambert, W.J., Aharon, P., 2011. Controls on dissolved inorganic carbon and $\delta^{13}C$ in cave waters from DeSoto Caverns: implications for speleothem $\delta^{13}C$ assessments. Geochim. Cosmochim. Acta 75, 753–768.
Lang, M., Faimon, J., Ek, C., 2015. The relationship between carbon dioxide concentration and visitor, numbers in the homothermic zone of the Balcarka Cave (Moravian Karst) during a period of limited ventilation. Int. J. Speleol. 44, 167–176.
Lang, M., Faimon, J., Godissart, J., Ek, C., 2017. Carbon dioxide seasonality in dynamically ventilated caves: the role of advective fluxes. Theor. Appl. Climatol. 129, 1355–1372.
Lechleitner, F.A., Amirnezhad-Mozhdehi, S., Columbu, A., Comas-Bru, L., Labuhn, I., Pérez-Mejías, C., Rehfeld, K., 2018. The potential of speleothems from Western Europe as recorders of regional climate: a critical assessment of the SISAL database. Quaternary 1, 30.
Li, J.-Y., Li, T.-Y., 2018. Seasonal and annual changes in soil/cave air pCO_2 and the $\delta^{13}C_{DIC}$ of cave drip water in response to changes in temperature and rainfall. Appl. Geochem. 93, 94–101.
Li, T.-Y., Shen, C.-C., Li, H.-C., Li, J.-Y., Chiang, H.-W., Song, S.-R.L., Yuan, D.-X., Lin, C. D.-J., Gao, P., Zhou, L.-P., Wang, J.-L., Ye, M.-Y., Tang, L.-L., Xie, S.-Y., 2011. Oxygen and carbon isotopic systematics of aragonite speleothems and water in Furong Cave, Chongqing, China. Geochim. Cosmochim. Acta 75, 4140e4156.
Li, T.-Y., Huang, C.X., Tian, L.J., Suarez, M., Gao, Y.L., 2018. Variation of $\delta^{13}C$ in plant-soil-cave systems in karst regions with different degrees of rocky desertification in southwest China. J. Cave Karst Stud. 80, 212–228.
Li, Y.D., Yang, Y., Jiang, X.Y., Zhao, J.Y., Sun, Z., Shi, X., Tian, N., Yang, Y.Y., Li, J.C., Duan, J.W., 2021. The transport mechanism of carbon isotopes based on 10 years of cave monitoring: implications for paleoclimate reconstruction. J. Hydrol. 592, 125841.
Liñán, C., Ojeda, L., Benavente, J., del Rosal, Y., Vadillo, I., Carrasco, F., 2020. Coupling air temperature records and gravimetric data to interpret ventilation patterns in a Mediterranean karstic system (Nerja-Pintada caves, southern Spain). Sci. Total Environ. 730, 139147.
Liñán, C., Jiménez de Cisneros, C., Benavente, J., Vadillo, I., del Rosal, Y., Ojeda, L., 2023. Coronavirus pandemic: an opportunity to study the anthropogenic impact on micro-climate conditions and $CaCO_3$ crystal morphology in the Nerja Cave (SE Spain). Sci. Total Environ. 883, 163693.
Liu, Z.H., Liu, X.L., Liao, C.J., 2008. Daytime deposition and nighttime dissolution of calcium carbonate controlled by submerged plants in a karst spring-fed pool: insights from high time-resolution monitoring of physico-chemistry of water. Environ. Geol. Water Sci. 55, 1159–1168.
Liu, Z.H., Wolfgang, D., Wang, H.J., 2010. A new direction in effective accounting for the atmospheric CO_2 budget: considering the combined action of carbonate dissolution, the global water cycle and photosynthetic uptake of DIC by aquatic organisms. Earth-Sci. Rev. 99, 162–172.
Luo, W.J., Wang, S.J., 2009. Transmission of $\delta^{13}C$ signals and its paleoclimatic implications in Liangfeng Cave system of Guizhou Province, SW China. Environ. Earth Sci. 59, 655–661.
Mattey, D., Lowry, D., Duffet, J., Fisher, R., Hodge, E., Frisia, S., 2008. A 53 year seasonally resolved oxygen and carbon isotope record from a modern Gibraltar speleothem: reconstructed drip water and relationship to local precipitation. Earth Planet. Sci. Lett. 269, 80–95.
Mattey, D., Atkinson, T.C., Barker, J.A., Fisher, R., Latin, J.P., Durell, R., Ainsworth, M., 2016. Carbon dioxide, ground air and carbon cycling in Gibraltar karst. Geochim. Cosmochim. Acta 184, 88–113.
Mattey, D., Atkinson, T.C., Hoffmann, D.L., Boyd, M., Ainsworth, M., Durell, R., Latin, J. P., 2021. External controls on CO_2 in Gibraltar cave air and ground air: implications for interpretation of $\delta^{13}C$ in speleothems. Sci. Total Environ. 777, 146096.
Moreno, A., Stoll, H., Jiménez-Sánchez, M., Cacho, I., Valero-Garcés, B., Ito, E., Edwards, R.L., 2010. A speleothem record of glacial (25–11.6kyr BP) rapid climatic changes from northern Iberian Peninsula. Global Planet. Change 71, 218–231.
Nickerson, N., Risk, D., 2006. Keeling plots are non-linear in non-steady state diffusive environments. Biogeochem. Cycles 20 (3), 3029–3083.
Nie, Y., Sun, J., 2022. Moisture sources and transport for extreme precipitation over Henan in July 2021. Geophys. Res. Lett. 49, e2021GL097446.
Oster, J.L., Montañez, I.P., Kelley, N.P., 2012. Response of a modern cave system to large seasonal precipitation variability. Geochim. Cosmochim. Acta 91, 92–108.
Pu, J.B., Wang, A.Y., Yin, J.J., Shen, L.C., Yuan, D.X., 2017. PCO_2 variations of cave air and cave water in a subtropical cave, SW China. Carbonates Evaporites 33, 477–487.
Riechelmann, D., Schröder-Ritzrau, A., Scholz, D., Fohlmeister, J., Spötl, C., Richter, D. K., Mangini, A., 2011. Monitoring Bunker Cave (NW Germany): a prerequisite to interpret geochemical proxy data of speleothems from this site. J. Hydrol. 409, 682–695.
Riechelmann, S., Schröder-Ritzrau, A., Spötl, C., Riechelmann, D.F.C., Richter, D.K., Mangini, A., Frank, N., Breitenbach, S.F.M., Immenhauser, A., 2017. Sensitivity of Bunker Cave to climatic forcings highlighted through multi-annual monitoring of rain-, soil-, and dripwaters. Chem. Geol. 449, 194–205.
Rudzka, D., McDermott, F., Baldini, L.M., Fleitmann, D., Moreno, A., Stoll, H., 2011. The coupled $\delta^{13}C$-radiocarbon systematics of three Late Glacial/early Holocene speleothems; insights into soil and cave processes at climatic transitions. Geochim. Cosmochim. Acta 75, 4321–4339.
Schoeller, D.A., Klein, P.D., Watkins, J.B., Heim, T., Maclean, W.C., 1980. ^{13}C abundances of nutrients and the effect of variations in ^{13}C isotopic abundances of test meals formulated for $^{13}CO_2$ breath tests. Am. J. Clin. Nutr. 33, 2375–2385.
Spötl, C., Fairchild, I.J., Tooth, A.F., 2005. Cave air control on dripwater geochemistry, Obir Caves (Austria): implications for speleothem deposition in dynamically ventilated caves. Geochim. Cosmochim. Acta 69, 2451–2468.
Sun, Z., Yang, Y., Zhao, J.Y., Tian, N., Feng, X.X., 2018. Potential ENSO effects on the oxygen isotope composition of modern speleothems: observations from Jiguan Cave, central China. J. Hydrol. 566, 164–174.
Tooth, A.F., Fairchild, I.J., 2003. Soil and karst aquifer hydrological controls on the geochemical evolution of speleothem-forming drip waters, Crag Cave, southwest Ireland. J. Hydrol. 273, 51–68.
Treble, P.C., Fairchild, I.J., Griffiths, A., Baker, A., Meredith, K.T., Wood, A., McGuire, E., 2015. Impacts of cave air ventilation and in-cave prior calcite precipitation on Golgotha Cave dripwater chemistry, southwest Australia. Quat. Sci. Rev. 127, 61–72.
Wu, Z., Zhang, C., Jiang, Z., Luo, W., Zeng, F., 2019. Advance of karst critical zone and its carbon cycle. Adv. Earth Sci. 34, 488 (In Chinese).
Yin, J.-J., Tang, W., Wang, Z., Pu, J., Lan, G., Yang, H., Wu, X., Li, J., 2021. Deciphering the hydroclimatic significance of dripwater $\delta^{13}C_{DIC}$ variations in monsoonal China based on modern cave monitoring. J. Hydrol. 603, 126882.
Yuan, D., 2015. Scientific innovation in Karst resources and envirinment research field of China. Carsologica Sinica 34, 98–100 (in Chinese).
Zhang, J., Quay, P.D., Wilbur, D.O., 1995. Carbon isotope fractionation during gas water exchange and dissolution of CO_2. Geochim. Cosmochim. Acta 59, 107–114.
Zhang, H., Zhou, Z., Dong, H., Yan, L., Ding, S., Huang, J., Gong, X., Su, D., 2023. Seasonal variations of cave dripwater hydrogeochemical parameters and $\delta^{13}C_{DIC}$ in

the subtropical monsoon region and links to regional hydroclimate. Sci. Total Environ. 881, 163509.